Available online at www.sciencedirect.com
ScienceDirect
Earth and Planetary Science Letters 262 (2007) 175–184
EPSL
www.elsevier.com/locate/epsl

# A depleted, destabilized continental lithosphere near the Rio Grande rift

Teh-Ru Alex Song *, D.V. Helmberger

*Seismological Laboratory, Division of Geological and Planetary Sciences, California Institute of Technology, Pasadena, CA 91125, USA*

Received 13 April 2007; received in revised form 13 July 2007; accepted 16 July 2007
Available online 7 August 2007
Editor: R.D. van der Hilst

**Abstract**

Seismic waveform diffraction patterns reveal a 120 km thick slab-like anomaly with about 4% increases in both compressional and shear wave speed, extending down to nearly 600 km between the Rio Grande Rift and the western Great Plains in the southwestern United States. Monte Carlo simulations suggest that the most probable interpretation is a temperature anomaly of about −400 K with additions of olivine (11%), orthopyroxene (12%) and losses of clinopyroxene (−14%), garnet (−9%) relative to the adjoining mantle asthenosphere beneath the Rio Grande Rift. This sesimic anomaly, probably continental lithosphere, is cold and is as depleted as the Archean continental lithosphere. It was likely formed in the Proterozoic age but destabilized during the Cenozoic rifting of the Rio Grande Rift.


*Keywords:* waveform diffraction; finite difference; continental rift; lithospheric destabilization

## 1. Introduction: Craton stability and longevity

Primitive mantle is mainly composed of garnet peridotites (>3 GPa), where sthe dominant mineral modes are olivine (ol), orthopyroxene (opx), clinopyroxene (cpx) and garnet (gt). During high degrees of partial-melting, clinopyroxene and garnet are largely extracted into the melt and the residue is left with more olivine and orthopyroxene (Walter, 1998; Matasukage et al., 2005). Continental lithospheres are generally believed to form under high degrees of melting of mantle at depths over 100 km. They are also depleted in iron but considered neutrally buoyant because compositional buoyancy is compensated by density increase due to thermal contraction (Jordan, 1978, 1988; Poudjom Djomani et al., 2001). Although the buoyancy does not guarantee the stability of the cratonic lithospheres (Lenardic and Moresi, 1999; Lenardic et al., 2003), many Archean cratons (>2.5 Gyr) seem stable for billions of years probably because of their high viscosity, strength and isolation from subduction (Lenardic and Moresi, 1999; Lenardic et al., 2003). Younger continental lithospheres surrounding these ancient cratons, however, can undergo substantial disturbances. In many cases, lithospheric instability, delamination or detachment occurs where there is a large contrast in the lithospheric thickness, temperature or strength (Bird, 1979; King and Ristema, 2000; Pascal et al., 2002; Pourhiet et al., 2006). To understand the longevity of the Archean craton and underlying lithosphere, it is critical to

* Corresponding author. Now at Department of Terrestrial Magnetism, Carnegie Institution of Washington, DC 20015, USA.
*E-mail addresses:* asong@ciw.edu (T.-R.A. Song), helm@gps.caltech.edu (D.V. Helmberger).

0012-821X/$ - see front matter © 2007 Elsevier B.V. All rights reserved.
doi:10.1016/j.epsl.2007.07.052

investigate how the surrounding lithospheres behave, which can be revealed by detailed seismic modeling.

Recently, a PASSCAL experiment, the LA RISTRA Transect, was installed to investigate mantle structures crossing the Great Plains, the Rio Grande Rift and the Colorado Plateau in the southwestern United States (Fig. 1a). The Rio Grande Rift, one of the major continental rifts, has existed since the late Cenozoic and it separates the Proterozoic continental lithospheres of the Great Plains and the Colorado Plateau (Baldridge et al., 1991). This dense array provides unprecedented opportunity to explore the underlying structure and answer fundamental questions regarding to the longevity of the continental lithosphere.

As demonstrated by Song and Helmberger (in press), waveform distortion and amplitude systematics are very useful in delineating and obtaining robust estimates of the velocity gradient of the adjoining 'slab-like' fast anomaly and mantle asthenosphere. The term 'slab-like' is introduced primarily for the geometric reason where the fast anomaly is dipping to the southeast and it is not yet clear how far this anomaly extends laterally off the 1-D array. Therefore, Song and Helmberger (2007) have assumed that this 'slab-like' anomaly extends laterally off the 1-D array over a length scale of the Fresnel zone of a 6 s S wave. They analyzed P and S waveforms of the same event-receiver pairs and found $R = \delta \ln V_s / \delta \ln V_p$ of about 1.25 using the amplitude pattern as a measure of the goodness of fit between the data and synthetics. Moreover, they have attempted to use this $R$ ratio to infer the origin of the slab-like anomaly. They calculated $\Delta(V_p/V_s)$ based upon their preferred estimates of $\Delta V_s/V_s$ and $R$ ratio and used the relationship between $V_p/V_s$ and Mg# (Lee, 2003) to simultaneously determine the temperature contrast $\Delta T$ and $\Delta$Mg# across the slab-like anomaly. They found $\Delta T$ of about 310 K and $\Delta$Mg# of about 3 and suggested the slab-like anomaly is likely cold and depleted.

However, such a $R$ ratio seems a little too large to explain the waveform broadening of the P waves. Besides, it is not easy to fully characterize the depletion of the slab-like anomaly by the Mg# alone while the relationship between $V_p/V_s$ and Mg# (Lee, 2003) might not strictly hold at ambient mantle condition. Therefore, we attempt to use the experimental results on the effect of melt depletion to the density and velocity of fertile peridotites (Schutt and Lesher, 2006) and simultaneously consider changes in major minerals (olivine, orthopyroxene, clinopyroxene, garnet) during partial melting. In addition, we will use cross-correlation of waveforms

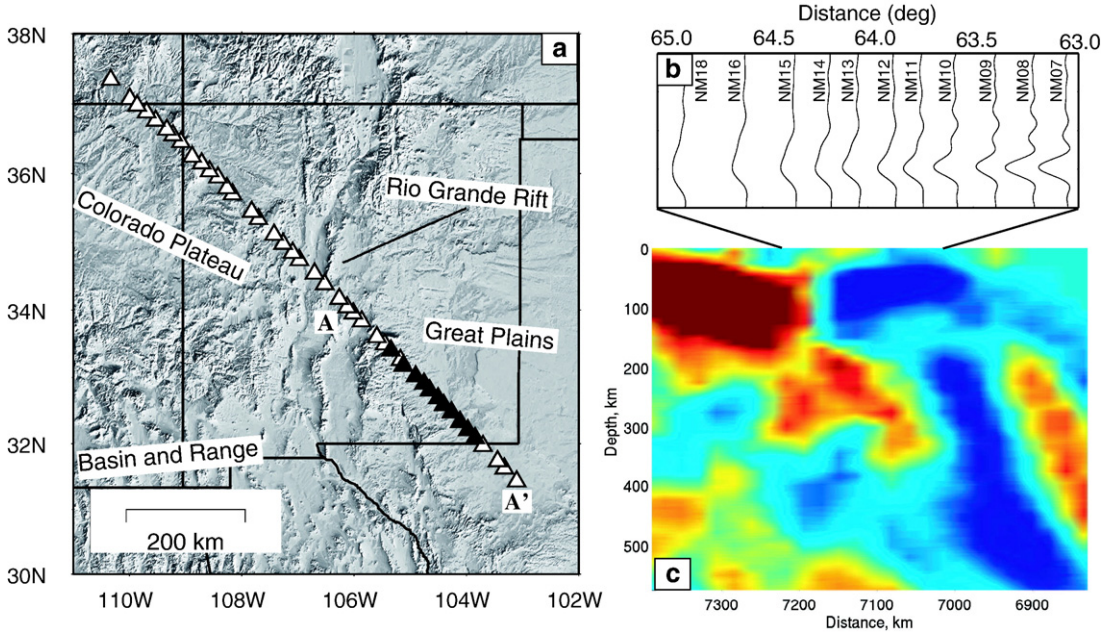


Fig. 1. Seismic waveform diffraction pattern along the LA RISTRA Transect. (a) Elevation map along with the LA RISTRA Transect (open triangles) crossing the edge of the Great Plains, the Rio Grande Rift and the Colorado Plateau. (b) Deconvolved S waveform section (event 990915, see also Table 1 in Song and Helmberger (in press)) showing waveform distortion across the transition between the western Great Plains and the Rio Grande Rift (solid triangles in (a)). Severe waveform broadening is present at stations toward the NW such as NM12-NM18. The S velocity section A–A' of model A extending down to 600 km is displayed in (c). It was constructed by amplifying existing tomographic model (Gao et al., 2004) and modeling S waveform data (Song and Helmberger, 2007, in press). The fast anomaly in the top 150 km beneath the western Great Plains is considered as the lithosphere.

between the data and synthetics as a measure of the goodness of fit, which is less affected by the site response. Instead of trying to obtaining a single estimate of temperature and compositional anomaly, we use Monte Carlo simulation to look for all possible estimates. In the following section, we will start by reviewing some relevant observations recorded along the LA RISTRA Transect, see Song and Helmberger (2007, in press) for detailed modeling.

## 2. Tomography, amplitude and waveform distortion

One of the most commonly used techniques in imaging the Earth's mantle is travel time tomography (Masters et al., 2000; Gao et al., 2004). However, it is usually necessary to damp and smooth these solutions, which makes interpretations difficult because the amplitude of velocity anomalies is less well constrained. Seismic waveform diffraction, on the other hand, is very useful in constraining the magnitude of seismic anomaly and its sharpness (Song and Helmberger, in press). It is generally associated with waveform distortions and amplitude decays as the wavefield goes through a large velocity contrast. We find systematic variations in waveform shapes and amplitudes recorded for events arriving from South America regardless of their locations and depths, but we do not observe such anomalous waveforms in other azimuths (Song and Helmberger, in press). Here we will explore waveform characteristics associated with the rapid changing lithospheric structure beneath the LA RISTRA Transect and make inferences on the origin of the observed seismic anomaly using Monte Carlo approaches. In general, our result is applicable to data recorded for other events as well (Song and Helmberger, in press).

We first show an example of a S waveform section recorded by the LA RISTRA Transect across the transition region between the Rio Grande Rift and the western Great Plains (Fig. 1a). We use the simplest wavelet from NM07 to remove the earthquake source effect. Array stations to the SE display nearly identical wavelets while S waveforms recorded at stations to the NW are distorted with smaller amplitudes (Fig. 1b). Note these diffraction phenomena are prominent at stations close to the fast-to-slow velocity boundary, where the slab-like anomaly is about 120 km wide and extends down to a depth of nearly 600 km (Fig. 1c).

Furthermore, these stations are situated directly above the slab-like anomaly suggesting that wave propagational effects are controlling the waveform shapes. Finite-difference synthetics (Vidale et al., 1985; Helmberger and Vidale, 1988) generated by propagating through the regional travel-time tomographic model (Gao et al., 2004) do not produce enough waveform distortions (Fig. 2). A new model A is constructed by amplifying the regional tomographic model so that it can explain travel time delays, amplitude decays and waveform distortions for records arriving from South

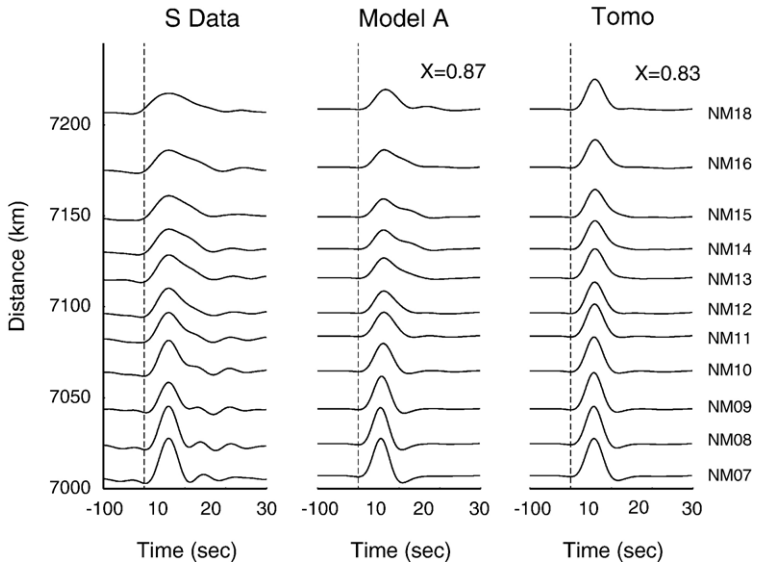


Fig. 2. Comparison of the observed waveforms (left) with synthetics. Synthetics computed with model A and tomography model are shown in the middle and right panels, respectively. Some amplitude and waveform broadening are present in the synthetics computed with tomographic model, but not strong enough. Both data and synthetics are band-pass filtered with corners at 0.01 Hz and 0.2 Hz. X indicates the average coefficient of cross-correlation between data and synthetics.

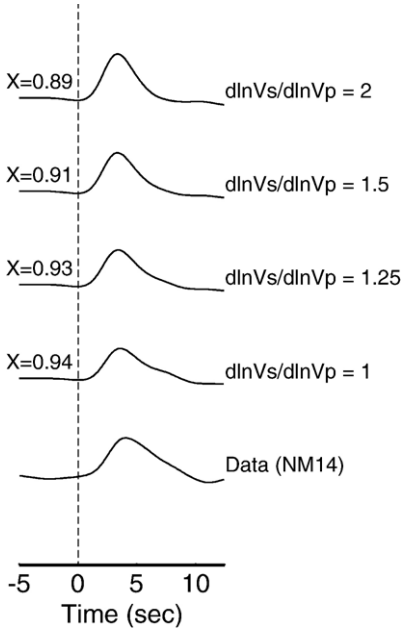


Fig. 3. Sensitivity of P waveform distortion to the scaling $R=\delta\ln V_s/\delta\ln V_p$. Synthetics are computed using $R$ of 2, 1.5, 1.25 and 1, respectively. When $R$ is about 1.5–2.0, there is no noticeable waveform distortions. P Waveform at NM14 is better explained with $R$ as low as 1. X indicates the average coefficient of cross-correlation between data and synthetics.

America events Song and Helmberger (in press). The geometry of the slab-like anomaly with a magnified velocity contrast across the fast-to-slow boundary is able to substantially distort the wavefronts and broaden the pulse widths. To characterize the origin of the anomalous structure, we further examine the P waveform section with identical source-receiver pairs.

They show almost exactly the same diffraction pattern as observed in the S waveform section (Figs. 3 and 4). Furthermore, the P waveform distortion is as profound as the S waveform, which indicates that the magnitudes of the P wave and S wave anomalies are similar. The scaling between the S wave and P wave anomaly $R=\delta\ln V_s/\delta\ln V_p$ has been discussed frequently to infer the origin of seismic anomalies (Masters et al., 2000; Karato and Karki, 2001).

Normally, $R$ is about 1.5−2.0 in the upper mantle when temperature is the dominant factor (Goes et al., 2000; Cammarano et al., 2003) since the shear modulus is much more affected by the temperature than the bulk modulus. Therefore, we will scale the S wave anomaly to P wave anomaly using a suite of scaling factors $R$ and test if temperature alone can explain the observations. However, synthetics computed from P velocity models using $R$ of 1.5−2.0 do not produce the observed P waveform distortions since the P wave velocity contrast appears too small (Fig. 3). It appears that the additional P waveform modeling proves invaluable in constraining the physical property of the observed seismic anomaly (Anderson and Bass, 1984).

To explain the P waveform section, it is important to consider compositional effects on seismic velocity. In particular, the effect of melt-depletion on seismic velocity has been recognized for mantle lithospheres, especially beneath ancient continents (Jordan, 1978). The most recognized relationship is between Mg#(Mg/Mg+Fe) and S wave velocity, where higher Mg# corresponds to increasing seismic velocity because of iron loss during mantle melting (Jordan, 1978; Lee, 2003). However, the relationship between Mg# and P wave velocity is less obvious (Lee, 2003). Recent melt experiments on fertile lherzolites provide a more detailed analysis on how melt-depletion effects seismic velocity (Schutt and Lesher, 2006). In particular, they obtain dependences of seismic velocity on mineral modes such as olivine, clinopyroxene and garnet at high pressures of 4–7 GPa (Schutt and Lesher, 2006). However, to account for processes other than partial melting, it is important to take orthopyroxene into account when characterizing continental peridotites (Boyd, 1989; Matasukage et al., 2005).

Traditionally, the relationship between Mg# and S wave velocity is used to infer how much the mantle lithosphere is depleted (Jordan, 1978; Lee, 2003) along with temperature anomaly. In this report, we intend to fully characterize the effect of mantle melting on seismic velocity considering changes in mineral phases and predict other quantities such as changes in density and Mg#. Specifically, we develop a simplified model that mimics model A and produces the same waveform distortions and amplitude decays as observed in the data (Song and Helmberger, in press). The average S wave anomaly of the slab-like anomaly is about $4\pm0.25\%$ with uncertainties related to the dip angle of the anomaly. Besides, we allow seismic esitmated $R$ ranging from 1.0−1.1, which accounts for possible noise in the data and the deconvolution process. These observations will be used in the following section to constrain the average temperature and compositional anomaly corresponding to the dipping structure.

## 3. Monte Carlo simulation

To explore possible changes in mineral modes, we perform Monte Carlo simulations to estimate velocity anomalies including parameters such as variations in temperature ($\Delta T$) and mineral modes of olivine ($\Delta$ol), orthopyroxene ($\Delta$opx), clinopyroxene ($\Delta$cpx) and garnet ($\Delta$gt) crossing the slab-like anomaly and the adjoining

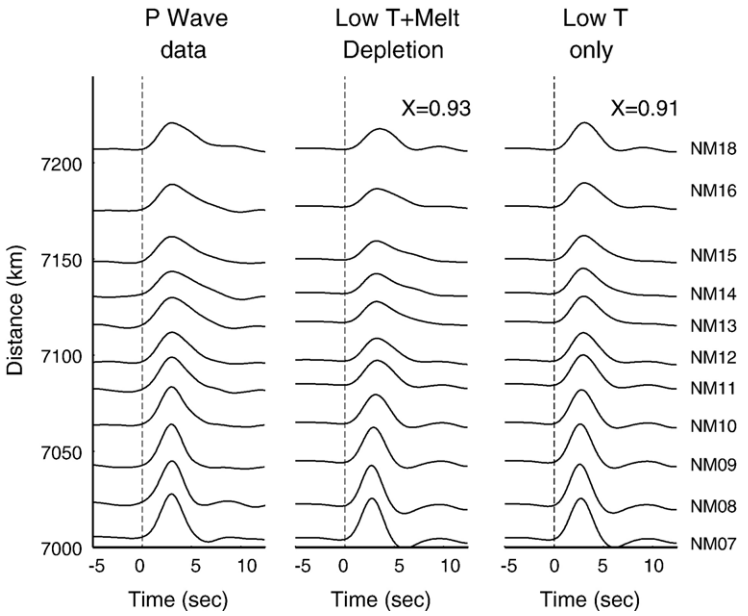


Fig. 4. Modeling of P waveform data. P waveforms are shown on the left panel with earthquake source effect removed using the simplest wavelet recorded at NM07. Synthetics computed considering temperature and melt-depletion induced compositional changes ($R=1$) are shown in the middle, while synthetics calculated considering only temperature ($R=1.5$) are not capable of explaining observations (right panel). X indicates the average coefficient of cross-correlation between data and synthetics. Both data and synthetics are band-pass filtered with corners at 0.01 Hz and 0.2 Hz.

mantle asthenosphere. The Monte Carlo simulation computes seismic anomaly for a given temperature anomaly ($\Delta T$) and compositional variations in olivine (ol), orthopyroxene (opx), clinopyroxene (cpx) and garnet (gt). The computed velocity anomaly (P or S) can be expressed as $\Delta V/V|_{\mathrm{cal}}=\Delta V/V|_T+\Delta V/V|_{\mathrm{com}}$, where $\Delta V/V|_T=\mathrm{d}\ln V/\mathrm{d}T\times\Delta T$; $\Delta V/V|_{\mathrm{com}}=\sum_{i=1}^{4}\mathrm{d}\ln V/\mathrm{d}M_i\times\Delta M_i$, where $M_{1,2,3,4}$ are olivine, orthopyroxene, clinopyroxene and garnet, respectively. Velocity derivatives of temperature and mineral modes are listed in Table 1.

We adopt velocity derivatives of four major mineral modes such as olivine, orthopyroxene, clinopyroxene and garnet based upon latest results from melting experiments and mineral physics data at 7 GPa (Table 1) (Matasukage et al., 2005; Schutt and Lesher, 2006). We correct for anelastic effects (Goes et al., 2000; Karato and Karki, 2001) on seismic velocity from temperature using $Q_s$ of 300 (Gudmunsson et al., 1994), which is appropriate for a fast continental lithosphere sampled by seismic waves at periods of 0.1–0.3 Hz. We allow a very small $R$ of 1.25 for temperature induced velocity anomaly and give a conservative estimate of compositional effects. Note the temperature effect on the velocity derivative due to anelastic relaxation is likely overestimated (Matas and Bukowinksi, 2007) and we possibly underestimate the temperature anomaly.

Using a larger $R$ from thermal anomaly would slightly modify our results on changes in mineral modes and temperature, but it does not change general estimates of increase in olivine and orthopyroxene and decrease in clinopyroxene and garnet. The temperature anomaly is apparently not much effected by the choice of $R$ since it depends primarily on the amplitude of S velocity anomaly. We produce similar result when implementing mineral physics data at lower pressure (4.5–6 GPa). Monte Carlo calculations are performed with temperature anomaly in the range of −520–0 K and changes

Table 1
Velocity and density dependence on temperature and composition (Matasukage et al., 2005; Schutt and Lesher, 2006) at 7 GPa

| | $\mathrm{d}\ln V_s/\mathrm{d}M$ | $\mathrm{d}\ln V_p/\mathrm{d}M$ | $\mathrm{d}\ln\rho/\mathrm{d}M$ |
|---|---|---|---|
| Temperature (K) | −0.00124 | −0.00124/R | $\alpha\Delta T$ |
| Olivine (ol)(%) (Schutt and Lesher, 2006) | −0.015 | 0.016 | −0.015 |
| Orthopyroxene (opx) (%) (Matasukage et al., 2005) | −0.046 | −0.059 | −0.008 |
| Clinopyroxene (cpx) (%) (Schutt and Lesher, 2006) | −0.008 | −0.062 | −0.016 |
| Garnet (gt) (%) (Schutt and Lesher, 2006) | 0.073 | 0.084 | 0.084 |

$\alpha$ is coefficient of thermal expansion $3\times10^{5}$ $\mathrm{K}^{-1}$ and $\Delta T$ is temperature anomaly. $R$ is $\mathrm{d}\ln V_s/\mathrm{d}\ln V_p$ estimated for temperature. The number within the parentheses gives the reference. The derivatives $\mathrm{d}\ln V_s/\mathrm{d}M$, $\mathrm{d}\ln V_p/\mathrm{d}M$ and $\mathrm{d}\ln\rho/\mathrm{d}M$ indicate the dependence of S velocity, P velocity and density on $M$, where $M$ is temperature, olivine, orthopyroxene, clinopyroxene or garnet.

in olivine, orthopyroxene, clinopyroxene and garnet of ±24%, respectively.

Only a subset of these simulations can explain the P and S waveform data simultaneously. In addition, it must also satisfy volumetric constraint $\Delta ol+\Delta opx+\Delta cpx+\Delta gt\equiv 0$ as well as partial-melting constraint where $\Delta ol$ and $\Delta opx$ go together as do $\Delta cpx$ and $\Delta gt$ (Walter, 1998; Lee, 2003; Matasukage et al., 2005; Schutt and Lesher, 2006). To analyze the subset of simulations that explain the P and S waveform data, we apply random sampling on the subset to simultaneously obtain the most probable estimate for each parameter. In each estimate of the model parameters such as temperature anomaly and compositional anomaly, we randomly select half of the models that explain seismic observation and then calculate the mean for each model parameter. We will present results based upon 4000 random samplings and the estimated temperature and compositional anomaly are very stable once the number of random sampling exceeds 500. To calculate density variation due to thermal contraction, we use coefficient of thermal coefficient $\alpha$ of $3\times10^{-5}$ $K^{-1}$.This $\alpha$ appears smaller than recent estimates on mantle peridotites (Lee, 2003; Schutt and Lesher, 2006). Therefore, we will have a lower estimate of the net buoyancy. A higher $\alpha$ of $3.5–4\times10^{-5}$ $K^{-1}$ can only strengthen our conclusion.

The total number of simulations is about $10^7$ while only a restricted set ($\sim10^3$) is able to explain the data. With additional compositional effects, we are able to reproduce observed P waveform distortion that is not

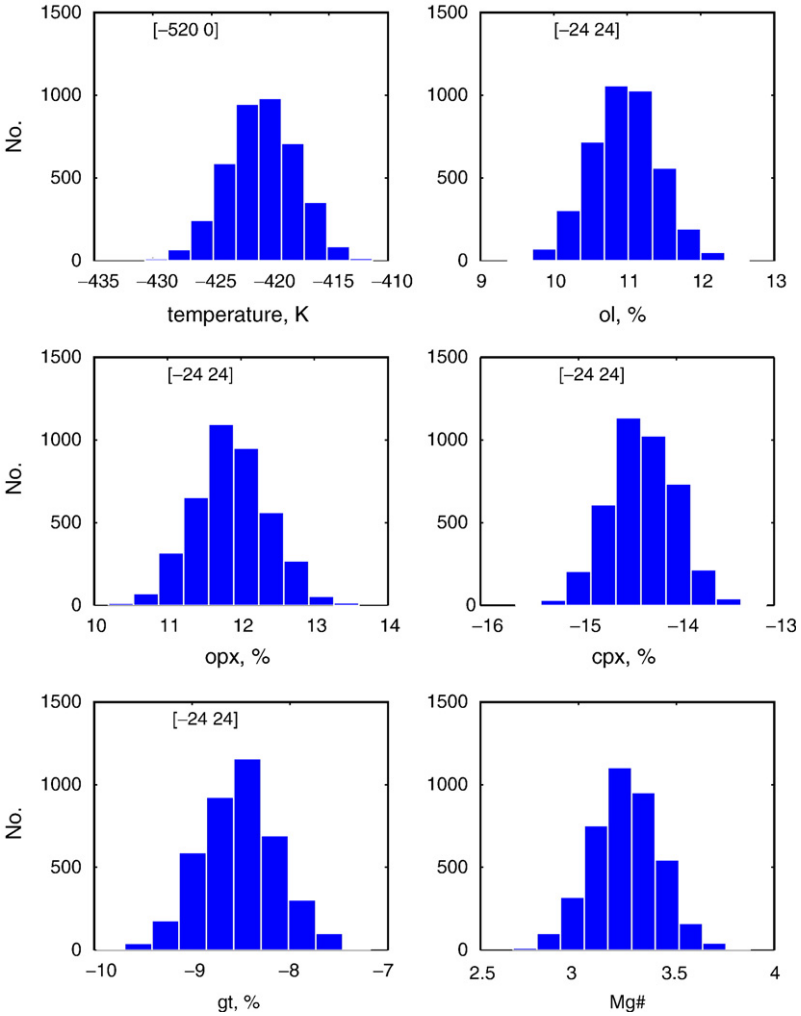


Fig. 5. Histograms of estimates on temperature anomaly and compositional changes in olivine (ol), orthopyroxene (opx), clinopyroxene (cpx), garnet (gt). Changes in Mg# are predicted according to density–Mg# relationship (Schutt and Lesher, 2006). The numbers within the brackets are the range of variations included in the Monte Carlo calculation.

able to be explained with temperature alone (Fig. 4). The most probable interpretation for the slab-like anomaly is a temperature decrease of about −420±30 K with additions of olivine (11±5%), orthopyroxene (12±5%) and losses of clinopyroxene (−14±3%), garnet (−9±4%) in comparison to the adjoining mantle asthenosphere beneath the Rio Grande Rift (Fig. 5).

We show that temperature is indeed the most dominant factor in producing the seismic anomaly, but the right balance among different mineral phases is critical in explaining the P and S waveform data simultaneously (Fig. 6). Increasing olivine and orthopyroxne effectively drops both P and S velocity while decreasing clinopyroxene and garnet slightly increases the P velocity but decreases the S velocity. This general trend of variations in these mineral modes is very consistent with xenolith estimates (Griffin et al., 1999; Poudjom Djomani et al., 2001; Lee, 2003; Griffin et al., 2004; O'Reilly and Griffin, 2006) and early mineralogical models of the upper mantle beneath the shield (Anderson and Bass, 1984). The composition of the slab appears to be that expected for a depleted continental lithosphere assuming the mantle asthenosphere adjoining the slab-like anomaly is fertile and composed of primitive peridotites (Table 2). We predict density anomaly $\Delta\rho_{com}/\rho$ of about −0.7±0.4% accociated with our estimates of compositional anomaly which corresponds to an iron loss of about 3.2±1.9% (equivalent to increasing Mg#) (Fig. 5) (Schutt and Lesher, 2006). This estimate of iron loss due to partial melting of garnet peridotites might depend on pressure while variations in these mineral phases are more robustly estimated (Fig. 7).

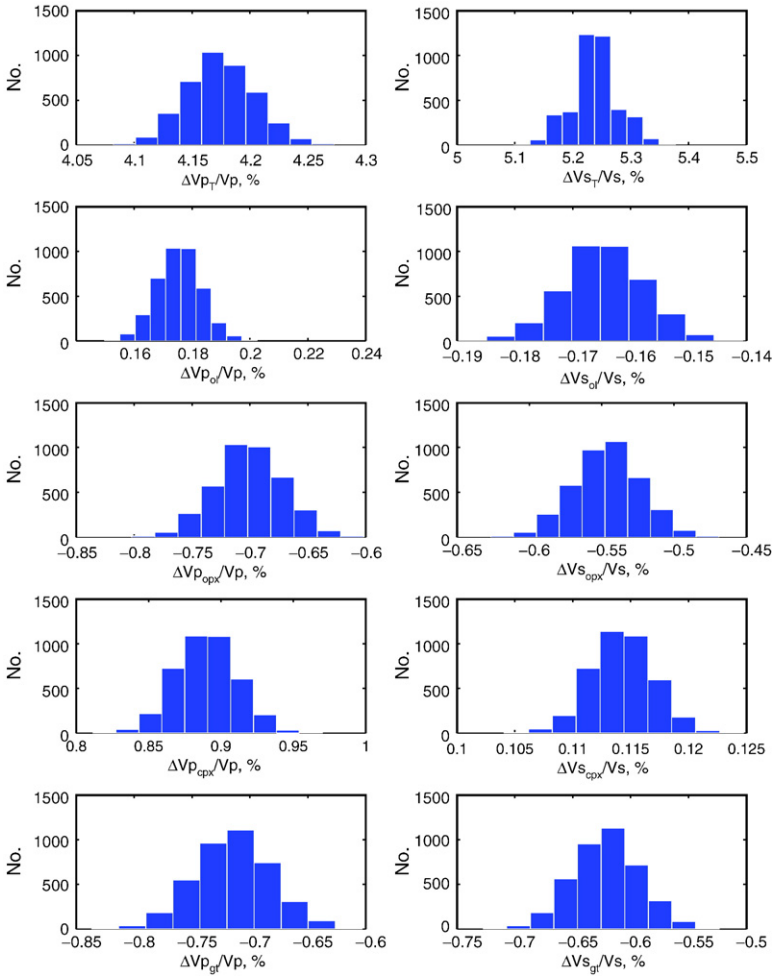


Fig. 6. Histogram of estimates on velocity anomalies due to temperature and composition. The left panel shows the estimated P wave anomaly due to temperature, olivine (ol), orthopyroxene (opx), clinopyroxene (cpx) and garnet (gt) and the right panel shows the estimated S wave anomaly due to temperature, olivine (ol), orthopyroxene (opx), clinopyroxene (cpx) and garnet (gt).

Table 2
Summary of seismological, petrological and geodynamic estimates of physical quantities related to continental lithospheres

| | ol/opx/cpx/gt | $\Delta\rho_{com}/\rho$ (%) | Mg# | $\Delta T$ (K) | $\delta\ln\rho/\delta\ln V_s$ |
|---|---|---|---|---|---|
| Primitive mantle (Poudjom Djomani et al., 2001) | 57/13/12/18 | 0 | 89.3 | | |
| Proterozoic xenoliths (Poudjom Djomani et al., 2001) | +13/+4/−6/−11 | −0.3 | +1.3 | | |
| Archean xenoliths (Poudjom Djomani et al., 2001) | +12/+12/−10/−14 | −0.8 | +3.4 | | |
| This study | +11/+12/−14/−9 | −0.7 | +3.2±1.9 | −420±30 | 0.1±0.1 |
| Geodynamic (Forte and Perry, 2000; Perry et al., 2003) | | | 1–2 | −400 | 0–0.1 |

Primitive mantle is considered as the reference and all other estimates are shown as relative perturbations.

We find the estimated temperature contrast $\Delta T$ of about 400 K is a bit larger than that estimated by Song and Helmberger (2007) (~310 K), while the estimate of $\Delta$Mg# is similar (~3).

## 4. Implications

We have shown that the dipping seismic anomaly constrained by waveform diffraction phenomena is much

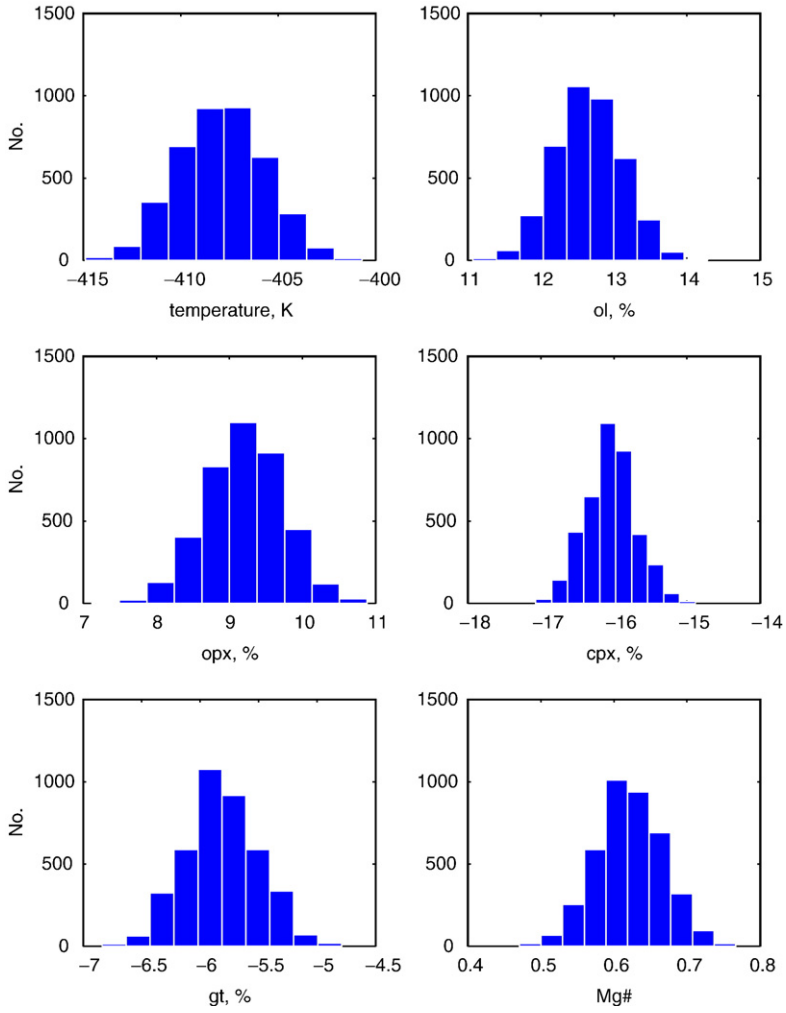


Fig. 7. Histograms of estimates on temperature anomaly and compositional changes in olivine (ol), orthopyroxene (opx), clinopyroxene (cpx), garnet (gt). Changes in Mg# are predicted according to density–Mg# relationship (Schutt and Lesher, 2006). 4000 random samplings are performed with half of the samples randomly chosen each time. Compositional effect on velocity and density is considered using estimates at 4 GPa (Schutt and Lesher, 2006). The small variation in Mg# is inferred based upon a much stronger effect of iron loss on density during melting at 4 GPa (Schutt and Lesher, 2006).

stronger than that shown in the tomographic model. More importantly, the relative amplitude between the S velocity anomaly and P velocity anomaly (or the scaling factor $R$) is better constrained, which justifies our inferences. Although the depleted lithosphere by itself is compositionally buoyant in comparison to the adjoining mantle asthenosphere, the temperature contrast reaches about −400 K and the net density contrast $\Delta\rho/\rho$ is 0.5±0.4%. The density-to-shear velocity scaling $\delta\ln\rho/\delta\ln V_s$ is found to be around 0.1±0.1, which is not inconsistent with geodynamic estimate $\delta\ln\rho/\delta\ln V_s$ of about 0.05 (Table 2) (Shapiro et al., 1999; Forte and Perry, 2000; Perry et al., 2003). Most strikingly, current estimated variations in the mineral modes such as olivine, orthopyroxene, clinopyroxene and garnet are more consistent with that estimated for the Archean xenoliths than that estimated for the Proterozoic xenoliths (Table 2). This strongly suggests that the observed cold, depleted lithosphere of the Proterozoic age (Griffin et al., 2004; O'Reilly and Griffin, 2006) can become unstable even if it is as depleted as the Archean lithosphere.

Our result is different from geodynamic modeling of long wavelength geoid, gravity and dynamic topography (Shapiro et al., 1999; Forte and Perry, 2000; Perry et al., 2003) where they conclude that large-scale cratons are in principle stable. While geochemical evidence has shown that the strength of the lithosphere is not directly related to its age but the degree of its depletion (Lee et al., 2001), our result suggests that lateral variations in temperature and buoyancy play an more important role. Lateral variation in lithospheric thickness can facilitate rifting (Pascal et al., 2002) and observed foundering of the continental lithosphere. While temperature contrast across the Rio Grande Rift and the western Great Plains is large, lithosphere removal might occur through delamination (Bird, 1979; Pourhiet et al., 2006), which can facilitate small scale convection (King and Ristema, 2000) or detachment of the depleted continental lithosphere. Further detail analysis on the elevation and history of vertical motions across the Colorado Plateau, the Rio Grande Rift and the western Great Plains is essential to examine the interaction between the Rio Grande Rift and the adjacent continental lithospheres.

We note the importance of using waveform and amplitude in constraining the magnitude of the velocity structure and drawing geophysical and geodynamic inferences. For instance, if S velocity anomaly of the dipping structure is only half of our estimate, as implied in the tomography model, we could expect a substantial underestimate of its temperature anomaly. Furthermore, the lack of P wave velocity anomaly in the tomographic model (Gao et al., 2004) can leads to the conclusion that temperature alone is able to explain the seismic anomaly. According to our estimate of iron loss (Schutt and Lesher, 2006), we can infer the degree of melting associated with this dipping anomaly of about 30±20%, If the melt fraction of 30% is responsible for producing the crust (~40–50 km) (Wilson et al., 2005) in the western Great Plains, it suggests that the lithosphere could reach depths of 150±20 km (Fig. 8), which is comparable with seismic constraints (Fig. 1c) (Gao et al., 2004). This result suggests that the recycling of the crust that might occur in the Archean craton (Rudnick, 1995; Schutt and Lesher, 2006) is likely not crucial to the Proterozoic crust of the western Great Plains. However, a damped velocity model might suggest a much lower degree of melting and the inference can become completely different (Fig. 8). As USArray and PASSCAL data become available and dense stations provide better spatial sampling, the use of waveform phenomena and amplitude systematics can then be routinely performed to better characterize seismic anomalies imaged by tomography and further

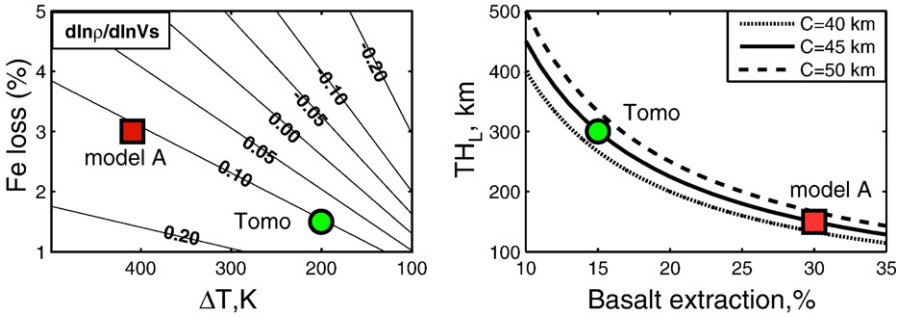


Fig. 8. Inference based on amplified model A and tomographic model. Left panel shows the inferred Fe loss based upon model A (red square) and tomographic model (green circle), respectively. The contours show the scaling between density and shear velocity, $\delta\ln\rho/\delta\ln V_s$. The basaltic melt fraction estimated from Fe loss (Schutt and Lesher, 2006) is shown on the right panel. Assuming the crust is made of these basaltic melts, the lithospheric thickness beneath the western Great Plains is about 300 km as inferred from the Fe loss (1.5%) estimated from tomography. Model A would predict a lithospheric thickness of about 150 km, which is similar to the seismic estimate.

improve the resolution of seismological findings and make self-consistent geophysical/geodynamic inferences.

## Acknowledgement

The authors would like to thank the editor Rob van der Hilst and an anonymous reviewer for their comments. This work was supported by the NSF-EAR-0639507 and contribution no. 8990 of the Division of Geological and Planetary Science, California Institute of Technology.

## References

Anderson, D., Bass, J., 1984. Mineralogy and composition of the upper mantle. Geophys. Res. Lett. 11, 637–640.

Baldridge, W.S., Perry, F., Vaniman, D., Nealey, L., Leavy, B.D., Laughlin, A.W., Kyle, P.R., Steintz, G., Gladney, E.S., 1991. Middle to late Cenozoic magmatism of the southeastern Colorado Plateau and central Rio Grande Rift (New Mexico and Arizona, U. S. A): a model for continental rifting. Tectonophysics 197, 327–354.

Bird, P., 1979. Continental delamination and the Colorado Plateau. J. Geophys. Res. 84, 7561–7571.

Boyd, F., 1989. Compositional distinction between oceanic and cratonic lithosphere. Earth Planet. Sci. Lett. 96, 15–26.

Cammarano, F., Goes, S., Vacher, P., Giardini, D., 2003. Inferring upper-mantle temperatures from seismic velocities. Phys. Earth Planet. Inter. 138, 197–222.

Forte, A., Perry, H., 2000. Geodynamics evidence for a chemically depleted continental tectosphere. Science 290, 1940–1944.

Gao, W., Grand, S., Baldridge, W.S., Wilson, D., West, M., Ni, J., Aster, R., 2004. Upper mantle convection beneath the central Rio Grande Rift imaged by P and S wave tomography. J. Geophys. Res. 109. doi:10.1029/2003JB002743.

Goes, S., Govers, R., Vacher, P., 2000. Shallow mantle temperatures under Europe from P and S wave tomography. J. Geophys. Res. 105, 11153–11169.

Griffin, W.L., O'Reilly, S.Y., Ryan, C., 1999. The composition and origin of sub-continental lithospheric mantle in mantle petrology: field observation and high-pressure experimentation: a tribute to Francies R. (Joe) Boyd. Geochem. Soc. 6, 13–45.

Griffin, W.L., O'Reilly, S.Y., Doyle, B.J., Person, N.J., Coopersmith, H., Kivi, K., Malkovets, V., Pokhilenko, N., 2004. Lithosphere mapping beneath the North American plate. Lithos 77, 873–922.

Gudmunsson, O., Kennett, B., Goody, A., 1994. Broadband observations of upper-mantle seismic phases in northern Australia and the attenuation structure in the upper mantle. Phys. Earth Planet. Inter. 84, 207–226.

Helmberger, D.V., Vidale, J., 1988. Modelling strong motioned produced by earthquakes with two-dimensional numerical codes. Bull. Seismol. Soc. Am. 78, 109–121.

Jordan, T., 1978. Composition and development of the continental tectosphere. Nature 274, 544–548.

Jordan, T., 1988. Structure and formation of the continental tectosphere. J. Petrol. 11–37 (Special issue).

Karato, S., Karki, B., 2001. Origin of lateral variation of seismic wave velocities and density in the deep mantle. J. Geophys. Res. 106, 21771–21783.

King, S., Ristema, J., 2000. African hot spot volcanism: small-scale convection in the upper mantle beneath cratons. Science 290, 1137–1140.

Lee, C.-T., 2003. Compositional variation of density and seismic velocities in natural peridotites at STP conditions: implications for seismic imaging of compositional heterogeneities in the upper mantle. J. Geophys. Res. 108. doi:10.1029/2003JB002413.

Lee, C.-T., Yin, Q., Rudnick, R.L., Jacobsen, S.B., 2001. Preservation of ancient and fertile lithospheric mantle beneath the southwestern United States. Nature 411, 69–73.

Lenardic, A., Moresi, L.N., 1999. Some thoughts on the stability of cratonic lithosphere: effects of buoyancy and viscosity. J. Geophys. Res. 104, 12747–12758.

Lenardic, A., Moresi, L.N., Muhlhaus, H., 2003. Longevity and stability of cratonic lithosphere: insights from numerical simulations of coupled mantle convection. J. Geophys. Res. 108. doi:10.1029/2002JB001859.

Masters, G., Laske, G., Bolton, H., Dziewonski, A., 2000. The relative behavior of shear velocity, bulk sound speed, and compressional velocity in the mantle: implications for chemical and thermal structure in Earth's deep interior: mineral physics and tomography from the atomic to the global scale. AGU Geophys. Monogr. 117, 63–88.

Matas, J., Bukowinski, M., 2007. On the elastic contribution to the temperature dependence of lower mantle seismic velocities. Earth Planet. Sci. Lett. 259, 51–65.

Matasukage, K., Nishihara, Y., Karato, S., 2005. Seismological signature of chemical differentiation of Earth's upper mantle. J. Geophys. Res. 110. doi:10.1029/2004JB003504.

O'Reilly, S.Y., Griffin, W.L., 2006. Imaging global chemical and thermal heterogeneity in the subcontinental lithospheric mantle with garnets and xenoliths: geophysical implications. Tectonophysics 416, 289–309.

Pascal, C., Van Wilk, J.W., Cloetingh, S., Davis, G., 2002. Effect of lithosphere thickness heterogeneities in controlling rift localization: numerical modeling of the Oslo Graben. Geophys. Res. Lett. 29. doi:10.1029/2001GL014354.

Perry, H., Forte, A., Eaton, D., 2003. Upper-mantle thermochemical structure below North America from seismic-geodynamic flow models. Geophys. J. Int. 154, 279–299.

Poudjom Djomani, Y., O'Reilly, S.Y., Griffin, W.L., Morgan, P., 2001. The density structure of subcontinental lithosphere through time. Earth Planet. Sci. Lett. 184, 605–621.

Pourhiet, L., Gurnis, M., Saleeby, J., 2006. Mantle instability beneath the Sierra Nevada Mountains in California and Death Valley extension. Earth Planet. Sci. Lett. 251, 104–119.

Rudnick, R., 1995. Making continental crust. Nature 378, 571–578.

Schutt, D., Lesher, C., 2006. Effects of melt depletion on the density and seismic velocity of garnet and spinel lherzolite. J. Geophys. Res. 111. doi:10.1029/2003JB002950.

Shapiro, S., Hager, B., Jordan, T., 1999. The continental tectosphere and Earth's long-wavelength gravity field. Lithos 48, 135–152.

Song, T.-R.A., Helmberger, D.V., 2007. P and S Waveform modeling of continental sub-lithospheric detachment at the eastern edge of the Rio Grande Rift. J. Geophys. Res. 112. doi:10.1029/2007JB004942.

Song, T.-R.A., Helmberger, D.V., in press. Validating tomographic model with broadband waveform modelling: an example from the LA RISTRATransect in the southwestern United States. Geophys. J. Int., doi:10.1111/j.1365-246X.2007.03508.x.

Vidale, J., Helmberger, D.V., Clayton, R., 1985. Finite difference seismograms for SH waves. Bull. Seismol. Soc. Am. 75, 1765–1782.

Walter, M., 1998. Melting of garnet peridotite and the origin of komatite and depleted lithosphere. J. Petrol. 39, 29–60.

Wilson, D., Aster, R., West, M., Ni, J., Grand, S., Gao, W., Baldridge, W.S., Semken, S., Patel, P., 2005. Lithospheric structure of the Rio Grande Rift. Nature 433, 851–855.